Computers and Mathematics with Applications 64 (2012) 1128–1139

Contents lists available at SciVerse ScienceDirect

Computers and Mathematics with Applications

journal homepage: www.elsevier.com/locate/camwa

DFT-based recursive group-harmonic energy distribution approach for power interharmonic identification

Hsiung-Cheng Lin [a,*], Liang-Yih Liu [b]

[a] Department of Electronic Engineering, National Chin-Yi University of Technology, Taichung 411, Taiwan

[b] Department of Automation Engineering, Chienkuo Technology University, Changhua 500, Taiwan

ARTICLE INFO

Keywords:
Harmonics
Interharmonics
Group harmonics
DFT

ABSTRACT

The Discrete Fourier Transform (DFT) is still a widely used tool for analyzing and measuring both stationary and transient signals in power system harmonics. However, the misapplications of DFT can lead to incorrect results caused by some problems such as the aliasing effect, spectral leakage and picket-fence effect. The strategy of a DFT-based recursive Group-harmonic Energy Distribution (GED) algorithm is developed for system-wide harmonic/interharmonic evaluation in power systems. The proposed algorithm can restore individual dispersing spectral leakage energy caused by the DFT, and thus retrieve respective real harmonic/interharmonic value. Every distribution of energy minimizing iteration procedure for harmonic/interharmonic evaluation can be convergent fast, and therefore guarantee each harmonic/interharmonic magnitude and respective frequency approaches its actual value. Consequently, not only can high precision in integer harmonic measurement be retained, but also the interharmonics can be identified accurately, particularly under system frequency drift. A numerical example is presented to verify the proposed algorithm in terms of robust, fast and precise performance.

1. Introduction

With increasing use of power electronic systems and time-variant non-linear loads in industry, the generated power harmonics and interharmonics have resulted in serious power line pollution. Power supply quality is therefore worsened. Traditional harmonics may cause negative effects such as signal interference, overvoltage, data loss, equipment malfunction, equipment heating and damage, etc. The noise on data transmission lines is also related to harmonics. For some special systems, harmonic current components may cause the effect of carrier signals, and thus interfere with other carrier signals. As a result, some facilities may be affected. Once a harmonic source enters computer instruments, the data stored in the computer may be lost. Moreover, harmonics may also cause transformer and capacitor overheating, thus reducing their working life. The resulting rotor heating and pulsating output torque will decrease the driver's efficiency [1–8].

The presence of power system interharmonics has not only brought many problems of harmonics but also produced additional problems. For instance, there are thermal effects, low frequency oscillation of mechanical systems, light and CRT flicker, interference of control and protection signals, high frequency overload of passive parallel filters, telecommunication interference, acoustic disturbance, saturation of current transformers, subsynchronous oscillations, voltage fluctuations, malfunctioning of remote control systems, erroneous firing of thyristor apparatus, loss of useful life of induction motors, etc. These phenomena may even happen under low amplitude [5,9–12].

* Corresponding author.
E-mail address: hclin@ncut.edu.tw (H.-C. Lin).

0898-1221/$ – see front matter © 2012 Elsevier Ltd. All rights reserved.
doi:10.1016/j.camwa.2012.03.031

Conventionally, the Discrete Fourier Transform (DFT) method is efficient for signal spectrum evaluation because of the simplicity and easy implementation. An improper use of DFT based algorithms can, however, lead to multiple interpretations of the spectrum [12–14]. For example, if the periodicity of the DFT data set does not match the periodicity of signal waveforms, the spectral leakage and picket-fence effect will occur. Since the power system frequency is subject to small random deviations, some degree of spectral leakage cannot be avoided. A number of algorithms, e.g., the short time Fourier Transform [15], least-square approach [16–18], Kalman filtering [19,20], and artificial neural networks [14,21], have been proposed to extract harmonics. The approaches may either suffer from low solution accuracy or less computational efficiency. None is reported to perform well in interharmonic identification under system frequency variations though each demonstrates its specific advantages.

The presence of interharmonics strongly poses difficulties in modeling and measuring the distorted waveforms. This is mainly due to: (1) very low values of interests of interharmonics (about one order of magnitude less than for harmonics), (2) the variability of their frequencies and amplitudes, (3) the variability of the waveform periodicity, and (4) the great sensitivity to the spectral leakage phenomenon. In recent years, the effect caused by interharmonics is being worsened apparently. Therefore, now the development of accurate interharmonic measurement has attracted great attention from both industry and academics. This is fully supported by exploring a number of publications (2008–2011) related to this field [22–33]. However, the published outcome may still suffer from low accuracy, long computational time, complexity or measurement limitation, etc. Accordingly, it is still an essential research issue to be carried on in this field.

IEC 61000-4-7 established a well disciplined measurement method for harmonics/interharmonics. This standard recently has been revised to add methodology for measuring interharmonics [34]. The key to the measurement of both harmonics and interharmonics in the standard is the utilization of a 10 or 12 cycle sample window upon which to perform the Fourier transform. However, the spectrum resolution with 5 Hz is not sufficiently precise to reflect the practical interharmonic locations for both 50 and 60 Hz systems. This paper presents harmonic/interharmonic identification using a DFT-based GED approach which retains the merits of DFT analysis and extends to interharmonic identification under system frequency variation environments. This paper is organized as follows. Section 2 gives a background of the concept of system harmonic/interharmonic measurement. Section 3 presents the proposed GED algorithm. In Section 4, the model validation with a numerical example is demonstrated. Performance results under system frequency drift are included and discussed. Conclusions are given in Section 5.

2. Background of system harmonic/interharmonic measurement

2.1. Fundamental analysis of harmonic/interharmonic

Integral multiples of AC system fundamental frequency are defined as harmonics of voltage or current signals. On the other hand, interharmonics are non-integral multiples of the AC system fundamental frequency, defined by IEC-1000-2-1 as follows [35].

"Between the harmonics of the power frequency voltage and current, further frequencies can be observed which are not an integer of the fundamental. They can appear as discrete frequencies or as a wide-band spectrum".

The definition of harmonic/interharmonic is illustrated as follows.

(a) Harmonic: $f_h = h \times f$, where h is an integer and greater than 0.
(b) DC: $f_h = 0$ Hz ($f_h = h \times f$, where $h = 0$).
(c) Interharmonic: $f_i \neq h \times f$, where h is an integer and greater than 0.

Note that f is the fundamental power system frequency.

By Fourier theory, any repetitive distorted (non-sinusoidal) waveform $i_s(t)$ can be expressed as Fourier series of various sinusoidal frequencies (harmonics/interharmonics).

$$i_s(t) = \sum_{k=-\infty}^{\infty} I_s(k\omega_0) e^{jk\omega_0 t} \tag{1}$$

$$I_s(k\omega_0) = \frac{1}{T} \int_t^{t+T} i_s(t) e^{-jk\omega_0 t} dt \tag{2}$$

where $\omega_0 (= 2\pi/T = 2\pi f)$ is the fundamental angular frequency, and $I_s(k\omega_0)$ is the kth coefficient.

Suppose the waveform $i_s(t)$ is sampled as N discrete points using the sampling rate f_s. With the digital signal processing (DSP) technology, the continuous signal $i_s(t)$ can be converted to a discrete signal $i_s[n]$, and then can be transformed by DFT as

$$I_s[k] = \frac{1}{N} \sum_{n=0}^{N-1} i_s[n] W_N^{kn} \tag{3}$$

where $I_s[k]$ denotes the discrete Fourier transform of $i_s[n]$ at frequency f_k, i.e., $f_k = k/T$, and $W_N = \exp(j2\pi/N)$.

The inverse DFT, which allows us to recover the signal from its spectrum, is given by

$$i_s[n] = \sum_{k=0}^{N/2-1} I_s[k] W_N^{-kn}. \tag{4}$$

Assume $i_s[n]$ is the periodic waveform with a period (T), and the angular frequency resolution ($\Delta\omega$) is determined by the truncated signal length and defined as follows.

$$\Delta\omega = \frac{2\pi}{T}. \tag{5}$$

If the data sampling length is chosen as p ($p > 1$ and is an integer number) periods, $\Delta\omega$ can be rewritten as follows.

$$\Delta\omega = \frac{2\pi}{pT} = \frac{\omega_0}{p}. \tag{6}$$

According to Eq. (6), Δf can be expressed as

$$\Delta f = \frac{1}{pT} = \frac{1}{pN_sT_s} = \frac{1}{NT_s} = \frac{f_s}{N} \tag{7}$$

where $N_s \triangleq \frac{N}{p}$ and $T_s \triangleq \frac{1}{f_s}$.

For instance, choose 10 60-Hz signal cycles for Fourier transform, and $\Delta f = 60/10 = 6$ Hz. Accordingly, 6, 12, 18 Hz,..., will appear in the spectrum, known as interharmonics. Furthermore, the executed time is $T_f = N \cdot \frac{1}{f_s}$ if the signal is sampled at N points by sampling rate f_s. Therefore, the Fourier fundamental period is expressed as T_f, i.e., $T_f = \frac{1}{\Delta f}$.

2.2. The concept of group harmonic

The measurement of interharmonics is difficult with results depending on many factors. Based on the so-called "group" suggested by IEC 61000-4-7, the concept of group harmonic is introduced as follows [35].

By the Parseval relation in its discrete form, the power of the waveform, P, can be expressed as [36,37]

$$P = \frac{1}{N} \sum_{n=0}^{N/2-1} i_s[n]^2 = \sum_{k=0}^{N/2-1} I_s[k]^2. \tag{8}$$

Both positive and negative values of spectral components are considered to transform the frequency dominant sampled signal into a periodic time dominant signal. Therefore, actual signal spectral components relevant to symmetrical frequencies are complex conjugates of each other. However, most real-world frequency analysis instruments display only the positive half of the frequency spectrum because the spectrum of a real-world signal is symmetrical around DC. Thus, the negative frequency information is redundant.

For this reason, the power at the discrete frequency f_k can be expressed as [37]

$$P[f_k] = I_s[k]^2 + I_s[N-k]^2 = 2I_s[k]^2 \tag{9}$$

where $k = 0, 1, 2, \ldots, N/2 - 1$.

In practice, only major harmonics including interharmonics are concerned to affect power systems. Consequently, $i_s(t)$ can be simply expressed as a certain series of sinusoidal harmonics, and the response to each harmonic can be thus determined by the following equation.

$$i_s(t) = \sum_{m=1}^{M} A_m \cos(\omega_m t + \phi_m) \tag{10}$$

where $\omega_m = 2\pi f_m$, $\phi_m = \tan^{-1}(-b_m/a_m)$ and $A_m = (a_m^2 + b_m^2)^{1/2}$.

With the sampling interval Δt to acquire either voltage or current waveform data in power systems, Eq. (10) is given in a discrete form as follows.

$$i_s[n] = \sum_{m=1}^{M} A_m \cos(\omega_m n\Delta t + \phi_m) \tag{11}$$

where n is the time step in the discrete sample sequence and $t = n\Delta t$.

The RMS value of the mth major harmonic amplitude located at the discrete frequency f_k is expressed as

$$A_m[f_k] = \sqrt{P[f_k]} = \sqrt{2} I_s[k] \tag{12}$$

where $m = 1, 2, \ldots, M$.

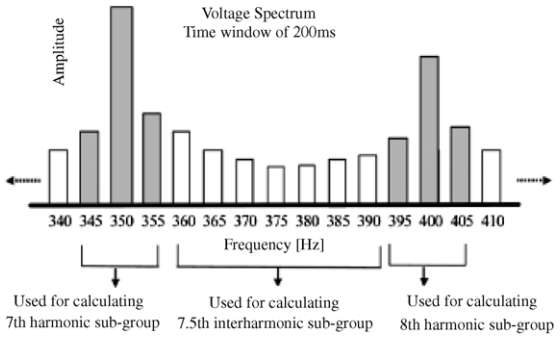

Fig. 1. IEC subgrouping of "bins" for both harmonics and interharmonics.
Source: Graph reproduced from [5].

The power of the mth harmonic at f_k may disperse over a frequency band around f_k due to the spectral leakage. Hence, the total power of harmonics within the adjacent frequencies around f_k can be restored into a "group power" [13]. Each "group power", i.e., $P^*_m[f_k]$, can be collected between $f_{k-\Delta k}$ and $f_{k+\Delta k}$ as follows.

$$P^*_m[f_k] = \sum_{\Delta k=-\tau}^{+\tau} (A_m[f_{k+\Delta k}])^2 \tag{13}$$

where τ is an integer number and denotes the group bandwidth.

Each harmonic amplitude can be estimated as

$$A^*_m[f_k] = \sqrt{P^*_m[f_k]}. \tag{14}$$

An interesting way to view this phenomenon is to observe the DFT implementation, shown in Fig. 1. Most leakages can be collected into one group and are considered as though they were all at the dominant harmonic frequency. The amplitude of interharmonics (and/or sub-harmonics) can be thus identified.

3. The group-harmonic energy distribution algorithm

3.1. The relation between sampling point and harmonic value

The power line waveform $s(t)$ (voltage/current) is sampled using the sampling rate $f_s(=1/T_s)$, which has the fundamental frequency f_d and its respective amplitude A_d, as follows.

$$s(n) = s(t)\,\big|_{t=nT_s}\ , \quad n = 0, 1, 2, \ldots, N-1 \tag{15}$$

where N is the sampled point of Fourier fundamental period T_f.

In general, the distorted signal can be composed of three parts, as follows.

$$s(n) = s_d(n) + s_h(n) + s_i(n) \tag{16}$$

where $s_d(n)$ is the fundamental component, $s_h(n)$ is the harmonic components, and $s_i(n)$ represents the interharmonic components.

Due to possible fundamental frequency drift, it may determine the new $\Delta f' = \frac{f_s}{N'}$ to find the correct fundamental frequency f'_d and its respective amplitude A'_d. Accordingly, the fundamental frequency signal $s'_d(n)$ and its harmonic signals $s'_h(n)$ can be obtained, as follows.

$$s'(n) = s(t)\left|_{t=\frac{n}{f'_s}} = s'_d(n) + s'_h(n) + s'_i(n), \quad n = 0, 1, 2, 3, \ldots, N'-1. \right. \tag{17}$$

Similarly, the same concept as above can be applied to the interharmonic evaluation in the distorted signal $s(n)$, assuming the major interharmonic component as the fundamental one and neglecting $s_d(n) + s_h(n)$, shown in Eq. (18). Therefore, the individual major interharmonic frequency f'_{ij} and its respective amplitude A'_{ij} can be found.

$$s''(n) = s(n) - [s_d(n) + s_h(n)] = s_i(n) = \sum_{j=1}^{m} s_{ij} \tag{18}$$

where m denotes the number of major interharmonics.

The length (N) of the sampled window for DFT analysis plays the critical role determinate if the spectrum can be achieved accurately. Based on the empirical observation using DFT, Fig. 2 indicates that the second stronger amplitude is found to be located at the right side of the dominant component, i.e., $A_m[f_{k+1}] > A_m[f_{k-1}]$, in the case of an overlong truncated window.

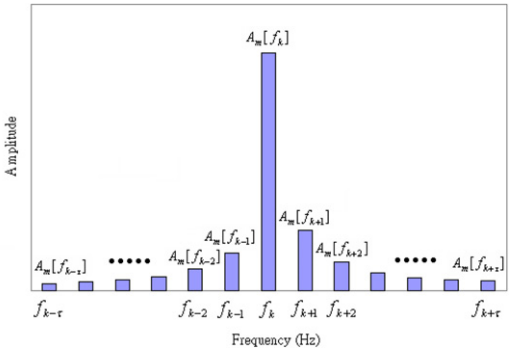

Fig. 2. Amplitude distribution around the dominant component.

In contrast, if the second stronger amplitude is located at the left side of the dominant component, i.e., $A_m[f_{k+1}] < A_m[f_{k-1}]$, the truncated-window length is insufficient for DFT analysis. Accordingly, the proposed GED approach is to develop the mechanism for correcting the window length according to the situation on the dispersed energy. This proposed GED method indeed extends the "group" concept that has been mentioned by IEC 61000-4-7 and some papers [5,13,37,38].

3.2. The proposed GED algorithm

The total dispersed energy, i.e., $P_m^{**}[f_k]$, around the dominant frequency is defined as

$$P_m^{**}[f_k] = \sum_{\Delta k=-\tau}^{+\tau} (A_m[f_{k+\Delta k}])^2 - (A_m[f_k])^2 \tag{19}$$

where it denotes the dispersed bandwidth energy, excluding the dominant component.

Based on the above concept, once the exact sampled window length (N) is found, $P_m^{**}[f_k]$ will reach the predefined minimum energy value ($P_{\min}$). To guarantee the convergence of $P_m^{**}[f_k]$ with the procedure repetition, N should be decreased if $A_m[f_{k+1}] > A_m[f_{k-1}]$, and N should be increased if $A_m[f_{k+1}] < A_m[f_{k-1}]$. The procedure will be repeated until the minimum energy value is achieved, more details shown in Fig. 3.

(1) Set $f_s = 5$ kHz, $N = 1000$.
(2) Sampling the line signal $i_s(t)$.
(3) Implement DFT.
(4) Determine the number (M) of major harmonics/interharmonics, and set $m = 1$.
(5) Implement DFT.
(6) If $A_m[f_{k+1}] > A_m[f_{k-1}]$, $N = N - 1$. Otherwise, go to next step.
(7) If $A_m[f_{k+1}] < A_m[f_{k-1}]$, $N = N+1$. Otherwise, go to next step.
(8) Check if $P_m^{**}[f_k] \leq P_{\min}$. If yes, the iteration loop stops and determines the updated N, i.e., N'. The major harmonic/interharmonic frequency f_m' and amplitude A_m' including the fundamental one can be thus obtained. Otherwise, go back to Step (5) to repeat the procedure until $P_m^{**}[f_k] \leq P_{\min}$.
(9) Let $m = m + 1$, $M = M - 1$, and $N = 1000$.
(10) Check whether $M = 0$. If yes, the iteration loop stops. Otherwise, go back to Step (5). Note that this iteration loop will continue until each major harmonic/interharmonic frequency f_m' and amplitude A_m' is found.

4. Model validation with a numerical example

The proposed GED algorithm has been tested by the synthesized line signal (voltage/current) to verify the effectiveness of harmonic/interharmonic analysis. The following example is used to illustrate the harmonic analysis of a distorted waveform [39,40,38].

$$\begin{aligned} s(t) = {} & \sin(2\pi f_d t + 37^\circ) + 0.3\sin(2\pi \cdot 3 \cdot f_d \cdot t + 78^\circ) + 0.2\sin(2\pi \cdot 5 \cdot f_d \cdot t - 19^\circ) \\ & + 0.25\sin(2\pi \cdot 131 \cdot t - 54^\circ) + 0.1\sin(2\pi \cdot 247.6 \cdot t + 62^\circ) + 0.15\sin(2\pi \cdot 391 \cdot t) \end{aligned} \tag{20}$$

where $f_d = 59.35$ Hz is the fundamental frequency.

As above, the line signal has a fundamental frequency, i.e., 59.35 Hz, with 0.65 Hz drift and a scaled amplitude of 1 V. The third and fifth harmonic components are included in the synthesized waveform to present a possible distorted waveform situation. Non-integer components, i.e., interharmonic, such as 131 Hz, 247.6 Hz, and 391 Hz are to be considered, reflecting a possible polluted line case. Note that the above harmonics/interharmonics are assigned different magnitudes and phases.

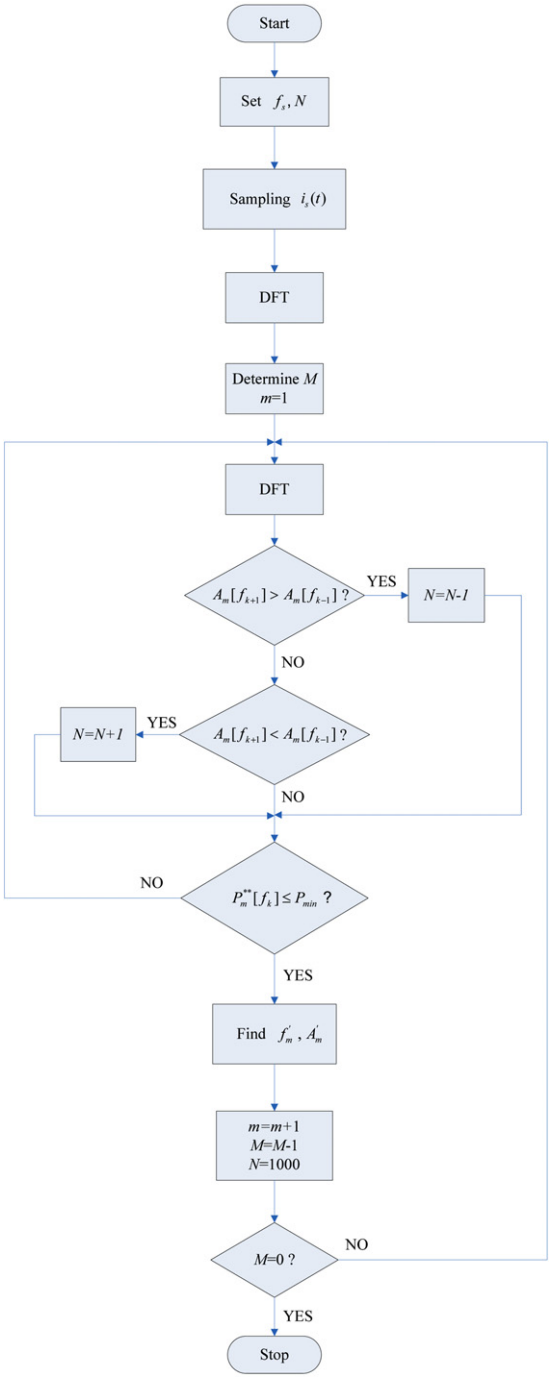

Fig. 3. The flowchart of the proposed GED algorithm.

4.1. Selection of group bandwidth (τ) and minimum energy value ($P_{\min}$)

We see that the larger group bandwidth (τ) can restore all leakages and regain the actual amplitude/frequency. However, with a large bandwidth the "group energy" may include considerable harmonic contents at distant frequencies because neighboring nominal harmonics may be dispersed widely. Additionally, the extracted frequency may be slightly apart from the actual value with a larger τ due to the influence of neighboring harmonic contents. As a consequence, the group bandwidth (τ) should be chosen as large as possible for obtaining an accurate amplitude but small enough to avoid the overlap between two neighboring harmonic groups. Based on the results by this proposed GED model, the group bandwidth (τ) is suggested to be chosen as $\tau = 4$ to reach the compromise.

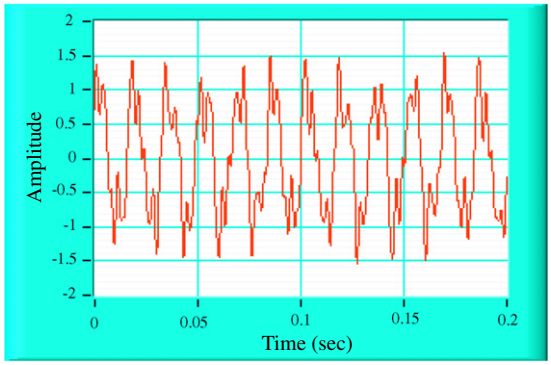

Fig. 4. The distorted waveform.

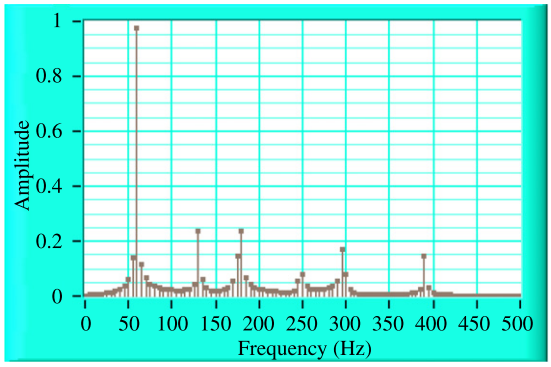

Fig. 5. Spectrum of the distorted waveform using DFT.

On the other hand, the minimum energy value ($P_{\min}$) is a crucial factor to stop the iteration loop of the proposed GED algorithm. Theoretically, $P_{\min}$ should be chosen as small as possible to achieve a more accurate result, but taking more iteration loops relatively. Therefore, $P_{\min}$ is set as 0.0001 with compromise in computational time, and the outcome is still satisfactory in this study.

4.2. Spectrum analysis

According to Eq. (20), we set $f_s = 5$ kHz, $N = 1000$, i.e., $\Delta f = 5$ Hz, and the waveform is shown in Fig. 4. As can be seen in Fig. 5, a considerable spectrum leakage occurs using DFT so that the result is unable to represent its actual spectrum.

Based on the proposed recursive GED algorithm, the following steps are illustrated to find the true harmonics/interharmonics.

Step (a): Measurement of fundamental and integer harmonics with a 0.65 Hz frequency drift

In this case, the fundamental frequency component including the third harmonic and fifth harmonic is considered to have a 0.65 Hz variation. The dispersed energy of the harmonics around the frequency band is significantly reduced from 0.0452 to 0.000385 within only 12 iteration loops, shown in Fig. 6. Fig. 7 indicates that each harmonic is approaching its true amplitude step by step. The amplitudes of fundamental, third and fifth components are thus obtained as 1.0, 0.29 and 0.2 at the 12th iteration loop from 0.977, 0.23 and 0.079 at the first iteration loop, respectively. Also, the fundamental frequency is found as 59.36 Hz, almost matching the true one.

Step (b): Measurement of the interharmonic at 131 Hz

In this stage, the dispersed energy of the interharmonic at 243.2 Hz is considerably reduced from 0.00833 to 0.0001 within eight iteration loops, shown in Fig. 8. Accordingly, its amplitude is obtained as 0.25 from 0.236 and the 131 Hz component is thus confirmed, shown in Fig. 9.

Step (c): Measurement of the interharmonic at 247.6 Hz

The dispersed energy of the interharmonic at 247.6 Hz is approaching zero from 0.0056 within nine iteration loops, shown in Fig. 10. Accordingly, its amplitude is obtained as 0.1 from 0.077 and the 247.6 Hz component is therefore confirmed, shown in Fig. 11.

Step (d): Measurement of the interharmonic at 391 Hz

In the last stage, the dispersed energy of the interharmonic at 391 Hz is going down quickly to 0.0001 from 0.00229 within only four iteration loops, shown in Fig. 12. As a result, its amplitude is obtained as 0.15 from 0.14 and the 391 Hz component is thus confirmed, shown in Fig. 13.

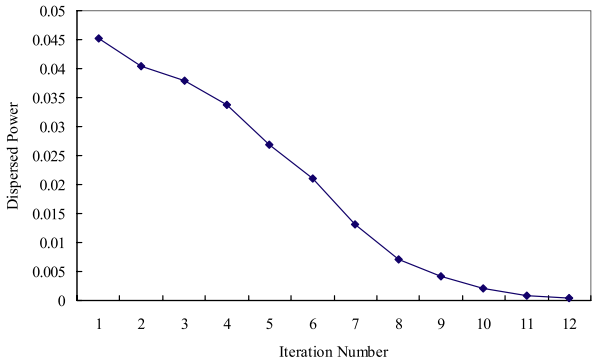

Fig. 6. Convergent curve of the dispersed energy at the harmonic components.

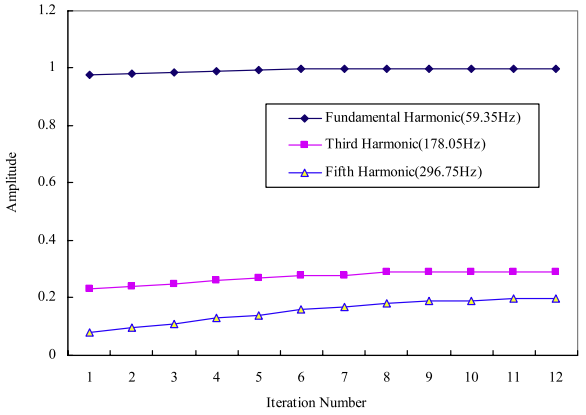

Fig. 7. Amplitude tracking curve of the harmonic components.

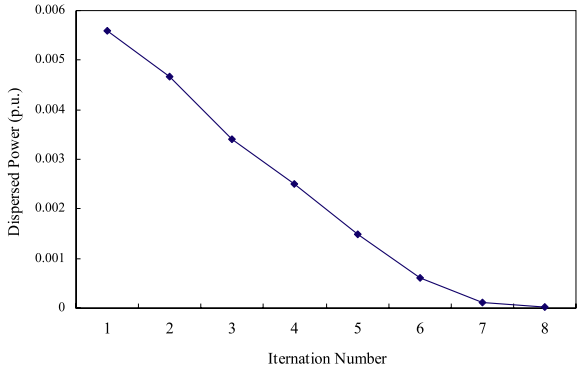

Fig. 8. Convergent curve of the dispersed energy at the 131 Hz interharmonic.

The waveform spectrum with the proposed recursive GED method is shown in Fig. 14. As can be seen, all dispersed energy surrounding the harmonics/interharmonics is almost completely restored so that the actual component amplitude and its respective frequency can be obtained accurately.

4.3. Comparison between DFT and GED analysis

The comparison between the DFT and the GED algorithm is listed in Tables 1–6, where τ is chosen as 4. Obviously, it is found that the dispersed amplitudes around the f_k, i.e., $f_{k-4} - f_{k-1}$ and $f_{k+1} - f_{k+4}$, are too apparent to be ignored by DFT. On the other hand, the proposed GED model can effectively reduce all dispersed energy to almost zero and thus guarantee true amplitudes/frequency to be achieved. Tables 1–3 indicate that the amplitudes of the fundamental, third harmonic and fifth harmonic at f_k by DFT are calculated as 0.98, 0.23 and 0.17, respectively. With the proposed GED method, their actual amplitudes can be obtained accurately as 1.0, 0.29, and 0.2. In Table 4, the amplitude of the 131 Hz interharmonic using

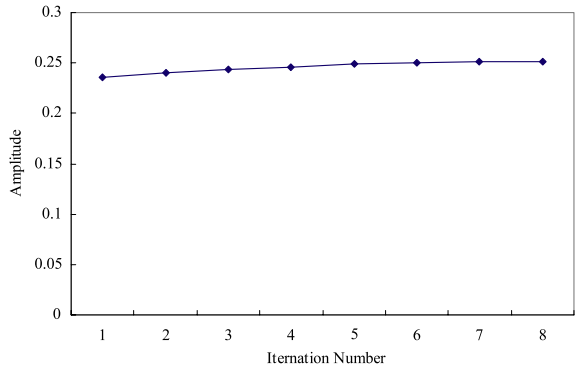

Fig. 9. Amplitude tracking curve of the 131 Hz interharmonic.

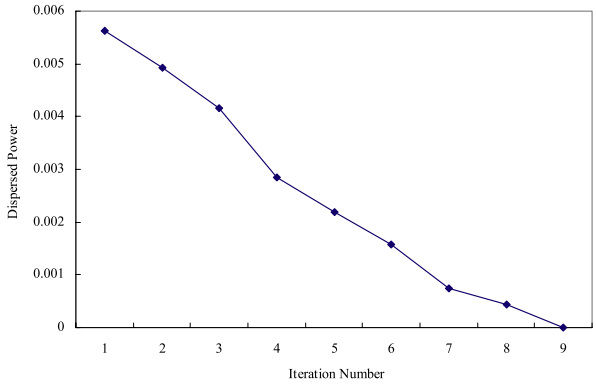

Fig. 10. Convergent curve of the dispersed energy at the 247.6 Hz interharmonic.

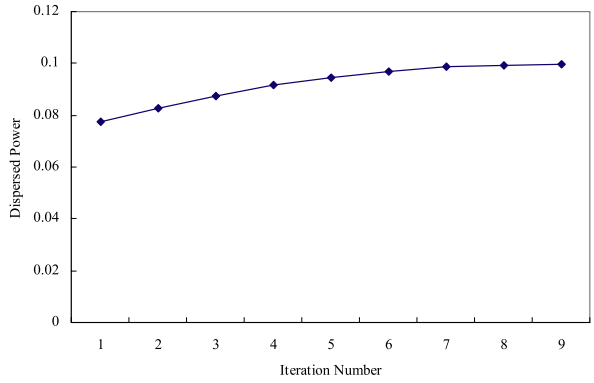

Fig. 11. Amplitude tracking curve of the 247.6 Hz interharmonic.

Table 1
Amplitude comparison of DFT and GED at $k = 12$ (fundamental harmonic).

kth	f_{k-4}	f_{k-3}	f_{k-2}	f_{k-1}	f_k	f_{k+1}	f_{k+2}	f_{k+3}	f_{k+4}
Real	0	0	0	0	1	0	0	0	0
DFT	0.027	0.038	0.062	0.14	0.98	0.12	0.064	0.045	0.035
GED	0.004	0.004	0.0046	0.005	1	0.0048	0.0055	0.006	0.0069

DFT at f_k is computed as 0.24, and the GED can achieve its actual value, i.e., 0.25. Similarly, Table 5 and 6 reveal that small distortion caused by 247.6 Hz and 391 Hz interharmonics at f_k can be accurately evaluated as 0.1 and 0.15 by the GED, respectively.

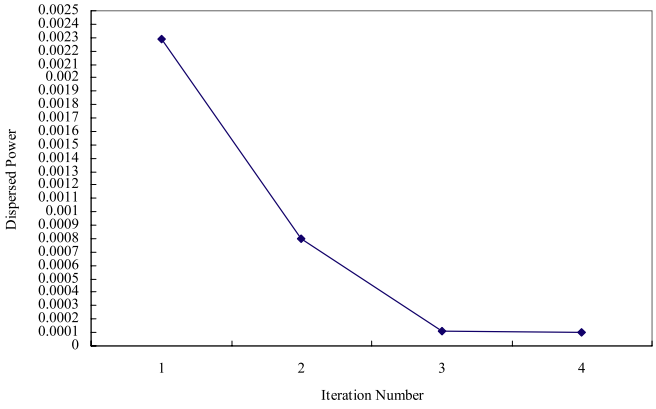

Fig. 12. Convergent curve of the dispersed energy at the 391 Hz interharmonic.

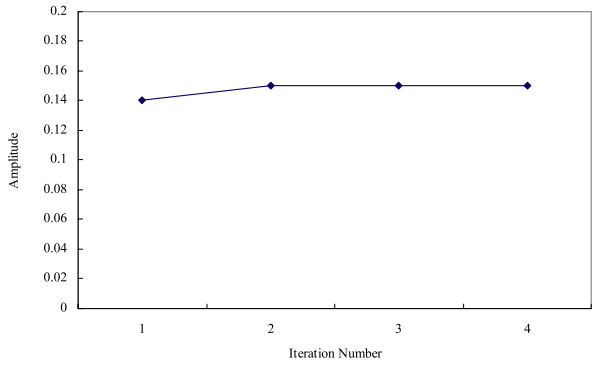

Fig. 13. Amplitude tracking curve of the 391 Hz interharmonic.

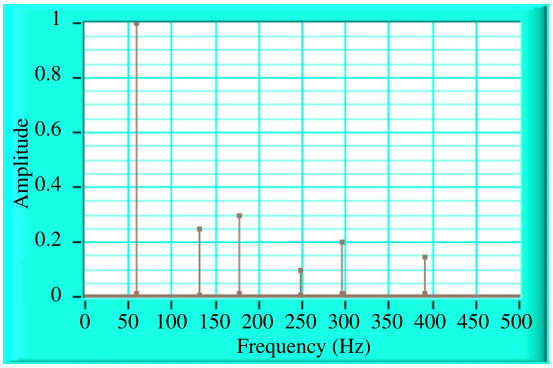

Fig. 14. Spectrum of the distorted waveform with GED.

Table 2
Amplitude comparison of DFT and GED at $k = 36$ (third harmonic).

kth	f_{k-4}	f_{k-3}	f_{k-2}	f_{k-1}	f_k	f_{k+1}	f_{k+2}	f_{k+3}	f_{k+4}
Real	0	0	0	0	0.3	0	0	0	0
DFT	0.023	0.032	0.052	0.14	0.23	0.069	0.042	0.031	0.025
GED	0.015	0.012	0.011	0.009	0.29	0.008	0.007	0.0067	0.006

Table 3
Amplitude comparison of DFT and GED at $k = 60$ (fifth harmonic).

kth	f_{k-4}	f_{k-3}	f_{k-2}	f_{k-1}	f_k	f_{k+1}	f_{k+2}	f_{k+3}	f_{k+4}
Real	0	0	0	0	0.2	0	0	0	0
DFT	0.025	0.028	0.035	0.052	0.17	0.079	0.026	0.014	0.0087
GED	0.0038	0.0035	0.0033	0.0029	0.2	0.0033	0.003	0.0028	0.0027

Table 4
Amplitude comparison of DFT and GED at $k = 26$ (131 Hz interharmonic).

kth	f_{k-4}	f_{k-3}	f_{k-2}	f_{k-1}	f_k	f_{k+1}	f_{k+2}	f_{k+3}	f_{k+4}
Real	0	0	0	0	0.25	0	0	0	0
DFT	0.021	0.022	0.027	0.043	0.24	0.058	0.027	0.02	0.018
GED	0.023	0.021	0.019	0.018	0.25	0.016	0.015	0.015	0.016

Table 5
Amplitude comparison of DFT and GED at $k = 49$ (247.6 Hz interharmonic).

kth	f_{k-4}	f_{k-3}	f_{k-2}	f_{k-1}	f_k	f_{k+1}	f_{k+2}	f_{k+3}	f_{k+4}
Real	0	0	0	0	0.1	0	0	0	0
DFT	0.013	0.013	0.016	0.052	0.078	0.035	0.027	0.025	0.024
GED	0.0047	0.005	0.005	0.006	0.1	0.0055	0.0052	0.0055	0.006

Table 6
Amplitude comparison of DFT and GED at $k = 78$ (391 Hz interharmonic).

kth	f_{k-4}	f_{k-3}	f_{k-2}	f_{k-1}	f_k	f_{k+1}	f_{k+2}	f_{k+3}	f_{k+4}
Real	0	0	0	0	0.15	0	0	0	0
DFT	0.009	0.011	0.015	0.026	0.14	0.033	0.013	0.008	0.0055
GED	0.004	0.0036	0.0027	0.0009	0.15	0.01	0.0076	0.0068	0.0063

5. Conclusions

Although the DFT has certain limitations in the harmonic analysis, it is still widely used in industry today. The harmonic/interharmonic identification using a DFT-based GED algorithm has been developed to be extracted accurately and efficiently. The test results confirm that the proposed recursive GED method can guarantee the tracking of each harmonic/interharmonic amplitude to be convergent at every iteration loop by the GED algorithm. There is no theoretical restriction in the locations of interharmonic components while the group bandwidth (τ) of each harmonic/interharmonic should be chosen appropriately. Moreover, the GED methodology has been implemented successfully by LabVIEW programming so that it can be easily extended to other software packages like microprocessor for on-line measurement. Additionally, the proposed GED can provide an advanced improvement for most measurement devices with some inherent errors because of the spectrum leakages caused by harmonics/interharmonics.

Acknowledgments

The financial support of this research by the National Science Council of the R.O.C., under Grant No. NSC 100-2221-E-167-001 is greatly appreciated.

References

[1] M.B. Rifai, T.H. Ortmeyer, W.J. McQuillan, Evaluation of current interharmonics from AC drives, IEEE Trans. Power Deliv. 15 (3) (2000) 1094–1098.
[2] Hao Qian, Rongxiang Ahao, Tong Chen, Interharmonics analysis based on interpolating windowed FFT algorithm, IEEE Trans. Power Deliv. 22 (2) (2007) 1064–1069.
[3] Quanming Zhang, Huijin Liu, Hongkun Chen, Qionglin Li, Zhenhuan Zhang, A precise and adaptive algorithm for interharmonics measurement based on iterative DFT, IEEE Trans. Power Deliv. 23 (4) (2008) 1728–1735.
[4] A. Testa, M.F. Akram, R. Burch, G. Carpinelli, G. Chang, V. Dinavahi, C. Hatziadoniu, W.M. Grady, E. Gunther, M. Halpin, P. Lehn, Y. Liu, R. Langella, M. Lowenstein, A. Medina, T. Ortmeyer, S. Ranade, P. Ribeiro, N. Watson, J. Wikston, W. Xu, Interharmonics: theory and modeling, IEEE Trans. Power Deliv. 22 (4) (2007) 2335–2348.
[5] H. Alasooly, M. Redha, Optimal control of UPFC for load flow control and voltage flicker elimination and current harmonics elimination, Comput. Math. Appl. 60 (4) (2010) 926–943.
[6] H. Alasooly, Comparison between optimal control strategies applied to a system with unified power flow controller, shunt converter and series converter, Comput. Math. Appl. 60 (4) (2010) 954–975.
[7] A. Beléndez, E. Arribas, M. Ortuño, S. Gallego, A. Márquez, I. Pascual, Approximate solutions for the nonlinear pendulum equation using a rational harmonic representation, Comput. Math. Appl. Corrected Proof, Available online 27 January 2012, in press (http://dx.doi.org/10.1016/j.camwa.2012.01.007).
[8] H.C. Lin, Fast tracking of time-varying power system frequency and harmonics using iterative-loop approaching algorithm, IEEE Trans. Ind. Electron. 54 (2) (2007) 974–983.
[9] D. Gallo, R. Langella, A. Testa, Interharmonics, part 1: aspects related to modeling and simulation, in: Sixth International Workshop on Power Definitions and Measurements under Non-Sinusoidal Conditions, Milano, 2003, pp. 168–173.
[10] D. Gallo, R. Langella, A. Testa, Interharmonics, part 2: aspects related to measurement and limits, in: Sixth International Workshop on Power Definitions and Measurements under Non-Sinusoidal Conditions, Milano, 2003, pp. 174–181.
[11] J. Barros, E. Prez, A. Pigazo, R.I. Diego, Simultaneous measurement of harmonics, interharmonics and flicker in a power system for power quality analysis, in: 2002. Fifth International Conference on Power System Management and Control, 2002, pp. 100–105.
[12] Masoud Karimi-Ghartemani, M. Reza Iravani, Measurement of harmonics/inter-harmonics of time-varying frequency, IEEE Trans. Power Deliv. 20 (1) (2005) 23–31.
[13] C.S. Moo, Y.N. Chang, Group-harmonic identification in power systems with nonstationary waveforms, IEE Proc. C 142 (5) (1995) 517–522.

[14] H.C. Lin, Intelligent neural network based adaptive power line conditioner for real-time harmonics filtering, IEE Proc. C 151 (5) (2004) 561–567.
[15] H.K. Kwok, D.L. Jones, Improved instantaneous frequency estimation using an adaptive short-time Fourier transform, IEEE Trans. Signal Process. 48 (10) (2000) 2964–2972.
[16] S.A. Soliman, R.A. Alammari, M.E. El-Hawary, M.A. Mostafa, Effects of harmonic distortion on the active and reactive power measurements in the time dominant: a single phase system, in: 2001 IEEE Power Tech. Proceedings, 2001, p. 6.
[17] M. Bettayeb, U. Qidwai, Recursive estimation of power system harmonics, Electr. Power Syst. Res. 47 (1998) 143–152.
[18] A. Al-Kandari, K.M. El-Naggar, Time dominant modeling and identification of nonlinear loads using discrete time-filtering estimator, in: 2003 IEEE Transmission and Distribution Conference and Exposition, 2003, pp. 126–131.
[19] A.A. Girgis, W.B. Chang, E.B. Makram, A digital recursive measurement scheme for on-line tracking of power system harmonics, IEEE Trans. Power Deliv. 6 (3) (1991) 1153–1160.
[20] J.A. Macias, A. Gomez, Self-tuning of kalman filters for harmonic computation, IEEE Trans. Power Deliv. 21 (1) (2006) 501–503.
[21] H.C. Lin, Intelligent neural network based fast power system harmonic detection, IEEE Trans. Ind. Electron. 54 (1) (2007) 43–52.
[22] H.C. Lin, Inter-harmonic identification using group-harmonic weighting approach based on the FFT, IEEE Trans. Power Electron. 23 (3) (2008) 1309–1319.
[23] Jing Yong, T. Tayjasanant, Wilsun Xu, Caixin Sun, Characterizing voltage fluctuations caused by a pair of interharmonics, IEEE Trans. Power Deliv. 23 (1) (2008) 319–327.
[24] G.W. Chang, C.I. Chen, Y.J. Liu, M.C. Wu, Measuring power system harmonics and interharmonics by an improved fast Fourier transform-based algorithm, IET Gener. Transm. Distrib. 2 (2) (2008) 193–201.
[25] I.Y.-H. Gu, Taekhyun Kim, E.J. Powers, W.M. Grady, A. Arapostathis, Detection of flicker caused by interharmonics, IEEE Trans. Instrum. Meas. 58 (1) (2009) 152–160.
[26] G.W. Chang, Chen Cheng-I, Liang Quan-Wei, A two-steage ADALINE for harmonics and interharmonics measurement, IEEE Trans. Ind. Electron. 56 (6) (2009) 2220–2228.
[27] Javier Valenzuela, Jorge Pontt, Real-time interharmonics detection and measurement based on FFT algorithm, Applied Electronics (2009) 259–264.
[28] Chen Cheng-I, G.W. Chang, Virtual instrumentation and educational platform for time-varying harmonic and interharmonic detection, IEEE Trans. Ind. Electron. 57 (2010) 3334–3342.
[29] A. Ramirez, The modified harmonic domain: interharmonics, IEEE Trans. Power Deliv. 26 (1) (2011) 235–241.
[30] Jian Cao, Tao Lin, Lin Liu, Jia-kai Ling, Xue-ling Huang, Power system interharmonics analysis based on new time frequency algorithm, in: 2011 Asia-Pacific Power and Energy Engineering Conference, APPEEC, 2011, pp. 1–3.
[31] A.B. Nassif, Y. Jing, H. Mazin, W. Xiaoyu, W. Xu, An impedance-based approach for identifying interharmonic sources, IEEE Trans. Power Deliv. 26 (1) (2011) 333–340.
[32] G.W. Chang, Shin-Kuan Chen, Huai-Jhe Su, Ping-Kuei Wang, Accurate assessment of harmonic and interharmonic currents generated by VSI-fed drives under unbalanced supply voltages, IEEE Trans. Power Deliv. 26 (2) (2011) 1083–1091.
[33] H.C. Lin, Power harmonics and interharmonics measurement using recursive group-harmonic power minimizing algorithm, IEEE Trans. Ind. Electron. 59 (2) (2012) 1184–1193.
[34] IEC 61000-4-7: Testing and measurement techniques: harmonics and interharmonics: general guide on harmonics and interharmonics measurements and instrumentation for power supply systems and equipment connected thereto, 2002.
[35] CEI/IEC 1000-2-1:1990, Electromagnetic compatibility, part 2: environment, sect. 1: description of the environment–electromagnetic environment for low-frequency conducted disturbances and signalling in public power supply systems, first ed., 1990-05.
[36] A.V. Oppenheim, R.W. Schafer, Discrete-Time Signal Processing, Prentice-Hall, 1989.
[37] William H. Press, Brian P. Flannery, Saul A. Teukolsky, William T. Vetterling, Numerical Recipes—the Art of Scientific Computing, Cambridge University Press, Cambridge, 1986, pp. 420–429.
[38] V.L. Pham, K.P. Wong, Wavelet-transform-based algorithm for harmonic analysis of power system waveforms, IEE Proc. C 146 (3) (1999) 249–254.
[39] H.C. Lin, C.S. Lee, Enhanced FFT based parametric algorithm for simultaneous multiple harmonics analysis, IEE Proc. C 148 (2001) 209–214.
[40] T.T. Nguyen, Parametric harmonic analysis, IEE Proc. C 144 (1) (1997) 21–25.